Time-Domain Electromagnetic Leaky Waves

Stumpf, Martin; Gu, Junhong; Lager, Ioan E.

DOI
10.1109/TAP.2023.3249358

Publication date
2023

Document Version
Final published version

Published in
IEEE Transactions on Antennas and Propagation

Time-Domain Electromagnetic Leaky Waves

Martin Štumpf, *Senior Member, IEEE*, Junhong Gu, *Student Member, IEEE*, and Ioan E. Lager, *Senior Member, IEEE*

***Abstract*— A causality preserving interpretation of the electromagnetic (EM) leaky-wave (LW) propagation in space and time is proposed for the first time. The Cagniard–deHoop (CdH) joint transform technique is applied for elucidating the relation between time-domain (TD) head waves (HWs), body waves (BWs), Cherenkov wave effects, and LWs. It is conjectured that the LW phenomenon in the TD is associated with a local maximum in the observed signal that occurs between the arrivals of the HW and BW constituents. A quantitative analysis that enables the space-time localization of the LW effect is performed theoretically and, then, illustrated via representative examples including the pulsed EM radiation from both a line source above a dielectric half-space, and narrow-slot antennas.**

***Index Terms*— Body wave (BW), Cagniard–deHoop (CdH) technique, Cherenkov radiation, head waves (HWs), leaky wave (LW), time-domain (TD) analysis.**

I. Introduction

LEAKY waves (LWs) can be viewed as nonmodal solutions (or noneigenmodes) of the source-free field equations in an open space. Owing to their improper physical behavior, LWs cannot exist on their own, but they can be utilized to represent the total field in a bounded subdomain of space [1]. Such solutions were dominantly investigated under the assumption of sinusoidally in time-varying fields, i.e., in the frequency domain (FD) (see [1], [2], [3], [4], [5], [6], [7], [8], [9], [10, Sec. 11.8]).

As far as the time-domain (TD) analysis of LW phenomena is concerned, the available literature on the subject is extremely scarce: Felsen and Niu [11] analyze dedicated joint-transform schemes to transform the terms of a hybrid ray-mode series expansion pertaining to the horizontal-electric-dipole excited fields inside a grounded slab. Next, Duffy [12] pursues a sophisticated analytical approach to replace a branch-cut integral by a sum of residue contributions corresponding to poles on a "nonphysically acceptable" Riemann sheet. A similar line of reasoning is also followed in [13], where both line- and point-source excited TD LWs in a grounded slab are analyzed in great detail. A very enlightening discussion in this respect can also be found in [14, Sec. 3.9], where TD LWs are first identified in the Laplace-transform domain expression for the 1-D plane-wave field reflected against a grounded slab and, subsequently, discussed in the context of line-source-excited head wave (HW) phenomena.

Inspired by the results in [12], [13], and [14], this article sets itself the task to offer for the first time a *causality preserving* interpretation of the electromagnetic (EM) LW propagation in *space and time*. Our framework hinges around conjecturing a relationship between HWs, body waves (BWs), LWs, and Cherenkov radiation effects. Since we programmatically aim at conceptual clarifications, we restrict ourselves to studying configurations that lend themselves to completely analytical handling. Our instrument of choice will be the Cagniard-deHoop (CdH) joint transform technique [15], [16], the inversion methodology that has been previously successfully used to explain and quantitatively describe the pseudo-Rayleigh-wave effect (also referred to as the Rayleigh LW) as observed along a fluid/solid planar interface [17], [18]. By this means we shall analyze the 2-D EM propagation in some canonical two-media configurations comprising a homogeneous, isotropic, dielectric domain embedded in free space.

After discussing some prerequisites, we shall first investigate the EM field due to an impulsive electric line source traveling with a constant velocity inside a dielectric half-space. Such a configuration may seem contrived from a practical point of view. Apart from being intrinsically relevant as an EM model for the Cherenkov radiation, it lays the conducive basis for developing the arguments that are central to our interpretation of the TD LW phenomenon. Subsequently, we shall examine a *stationary* line source located in a dielectric half-space, the analysis of the TD reflected field at the interface demonstrating a behavior that we associate with the TD LW phenomenon (see the detailed explanation on the used terminology in the Appendix). This phenomenon will also be observed in the case of the EM radiation from a 2-D slot-excited dielectric slab, where we analyze HW, LW, and BW contributions as they propagate by multiple reflections inside the slab. The final step will concern the study of the EM field propagating along an infinite slot in a perfectly electrically conducting (PEC) screen that separates a dielectric half-space from a free-space one. We end by drawing conclusions.

Manuscript received 22 August 2022; revised 22 January 2023; accepted 27 January 2023. Date of publication 2 March 2023; date of current version 7 April 2023. This work was supported by the Czech Science Foundation under Grant 20-01090S. The stay of MS at the THz Sensing Group, TU Delft, was financed by the Czech Ministry of Education, Youth and Sports under Project CZ.02.2.69/0.0/0.0/18_053/0016962. *(Corresponding author: Martin Štumpf.)*

Martin Štumpf is with the Lerch Laboratory of EM Research, Department Radioelectronics, Faculty of Electrical Engineering and Communication, Brno University of Technology, 616 00 Brno, Czech Republic (e-mail: martin.stumpf@centrum.cz).

Junhong Gu and Ioan E. Lager are with the THz Sensing Group, Faculty of Electrical Engineering, Mathematics and Computer Science, Delft University of Technology, 2628 CD Delft, The Netherlands (e-mail: j.gu-3@student.tudelft.nl; i.e.lager@tudelft.nl).

Color versions of one or more figures in this article are available at https://doi.org/10.1109/TAP.2023.3249358.

Digital Object Identifier 10.1109/TAP.2023.3249358

II. Definitions

Position in the analyzed problem configurations is specified by the coordinates $\{x, y, z\}$ with respect to an orthogonal Cartesian reference frame with the origin, $\mathcal{O}$, and the three base vectors $\{\boldsymbol{i}_x, \boldsymbol{i}_y, \boldsymbol{i}_z\}$. The time coordinate is denoted by t. The Dirac-delta distribution is denoted by $\delta(t)$ and the Heaviside unit-step function is represented by $\mathrm{H}(t)$.

To properly account for the universal property of causality, TD LWs will be analyzed with the aid of the CdH joint-transform technique that makes use of a unilateral Laplace transformation in combination with the wave-slowness (Fourier-type) representation [15]. To show the notation, we give the integral expressions for the y-component of the electric-field strength, $E_y(x, y, z, t)$. The Laplace transform can be then written as

$$\hat{E}_y(x, y, z, s) = \int_{t=0}^{\infty} \exp(-st) E_y(x, y, z, t) \mathrm{d}t \quad \text{for } \{s \in \mathbb{R}; s > 0\} \tag{1}$$

and the wave-slowness representation along the x-direction, for instance, can be expressed as

$$\hat{E}_y(x, y, z, s) = \frac{s}{2\pi \mathrm{i}} \int_{p=-\mathrm{i}\infty}^{\mathrm{i}\infty} \exp(-spx) \tilde{E}_y(p, y, z, s) \mathrm{d}p \tag{2}$$

where p is the (imaginary-valued) slowness parameter and s serves as a scaling parameter. If the problem configuration permits, a similar representation can also be taken along the y- or/and z-direction.

III. Impulsive Line Source Over a Half-Space

In this section, we shall examine the EM-field radiation from an impulsive line source in a two-medium configuration. More precisely, we shall analyze the TD *reflected* field due to a y-oriented, impulsive electric line source that is located at a height $h > 0$ in the upper half-space, say $\mathcal{D}_1 = \{-\infty < x < \infty, -\infty < y < \infty, z > 0\}$, whose EM properties are described by (scalar, real-valued and positive) electric permittivity ϵ_1 and magnetic permeability μ_0. Likewise, the EM properties of the lower half-space, $\mathcal{D}_0 = \{-\infty < x < \infty, -\infty < y < \infty, z < 0\}$, are described by ϵ_0 and μ_0 (see Fig. 1). The corresponding EM wave speeds in $\mathcal{D}_{0,1}$ are described by $c_{0,1} = (\mu_0 \epsilon_{0,1})^{-1/2} > 0$, respectively. We shall assume that the line source is located in a denser medium, i.e., $c_1 < c_0$.

In our analysis, we shall consider two cases. First, bearing in mind that the Cherenkov effect [19] is in the literature occasionally associated with LW phenomena (see [9], [20], [21], for example), we shall analyze the TD EM field associated with a *traveling* line source. In the second case, the same problem configuration is to be excited by a *fixed* line source. For detailed CdH analyses of TD EM-fields radiated from stationery and traveling line current sources in the presence of a dielectric half-space we refer the reader to [22] and [23], respectively.

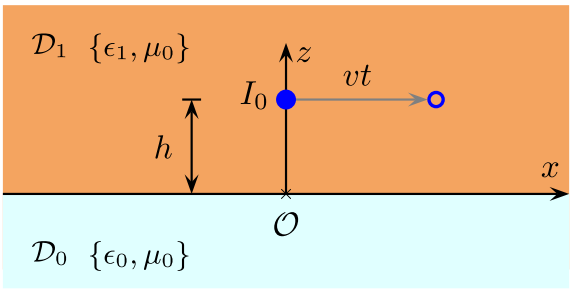

Fig. 1. Impulsive electric-line source above a half-space.

A. Traveling Line Source

First, we shall analyze the reflected field due to the electric-line source that travels in the positive x-direction along $z = h$ at a constant speed, say $v > 0$ (see Fig. 1). The latter is assumed to be higher than the wave speed in $\mathcal{D}_1$, but lower than c_0 corresponding to $\mathcal{D}_0$, i.e., $c_1 < v < c_0$. Assuming next, for simplicity, the unit-step temporal profile, the traveling line source can be defined via its electric-current volume density as

$$J_y(x, z, t) = I_0 \delta(x - vt) \delta(z - h) \mathrm{H}(t) \tag{3}$$

where I_0 (in A) denotes the electric-current amplitude. Since the problem configuration and the excitation source are y-independent, the nonvanishing (E-polarized) field components are $\{E_y, H_x, H_z\}(x, z, t)$. Those components that are tangential with respect to the (source-free) interface do meet the continuity-type conditions

$$\lim_{z \downarrow 0} \{E_y, H_x\}(x, z, t) = \lim_{z \uparrow 0} \{E_y, H_x\}(x, z, t) \quad \text{for all } x \in \mathbb{R} \text{ and } t > 0. \tag{4}$$

To solve the boundary-value problem, its general solution is traditionally written as the superposition of the incident and reflected fields, $E_y = E_y^{\mathrm{i}} + E_y^{\mathrm{r}}$ in $\mathcal{D}_1$, and as the (total) transmitted field in $E_y = E_y^{\mathrm{t}}$ in $\mathcal{D}_0$. Combining now the Laplace transformation (1) with the slowness representation (2), the corresponding reflected EM-field in the s-domain can be expressed via the following complex-slowness integral:

$$\hat{E}_y^{\mathrm{r}}(x, z, s) = \frac{\mu_0 I_0}{2\mathrm{i}\pi} \int_{p=-\mathrm{i}\infty}^{\mathrm{i}\infty} \exp\{-s[px + \gamma_1(p)(z + h)]\} \times \frac{\tilde{R}_\perp(p)}{vp - 1} \frac{\mathrm{d}p}{2\gamma_1(p)} \tag{5}$$

where the (transform-domain) reflection coefficient, $\tilde{R}_\perp(p)$, is expressed via the vertical slowness parameters, $\gamma_{0,1}(p)$, as

$$\tilde{R}_\perp(p) = [\gamma_1(p) - \gamma_0(p)]/[\gamma_1(p) + \gamma_0(p)] \tag{6}$$

$$\gamma_{0,1}(p) = \left(c_{0,1}^{-2} - p^2\right)^{1/2} \quad \text{with } \mathrm{Re}(\gamma_{0,1}) \geq 0. \tag{7}$$

The slowness integral can be transformed to the TD analytically via the standard CdH technique [15]. To that end, the integrand is first analytically continued away from the imaginary axis, while keeping $\mathrm{Re}(\gamma_{0,1}) \geq 0$ throughout the complex p-plane. This leads to the horizontal branch cuts along $\{c_{0,1}^{-1} \leq |\mathrm{Re}(p)| < \infty, \mathrm{Im}(p) = 0\}$. In addition,

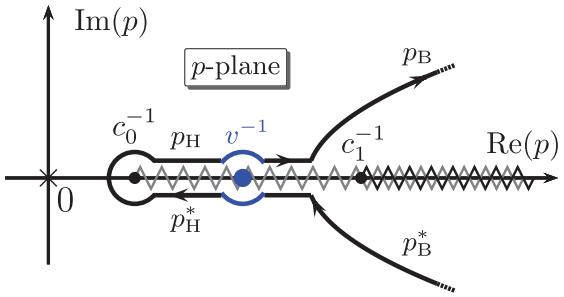

Fig. 2. CdH path in the complex p-plane pertaining to the reflected field above the half-space due to the *traveling* line source for $x > 0$. The gray and black zigzags represent the branch cuts originating at c_0^{-1} and c_1^{-1}, respectively.

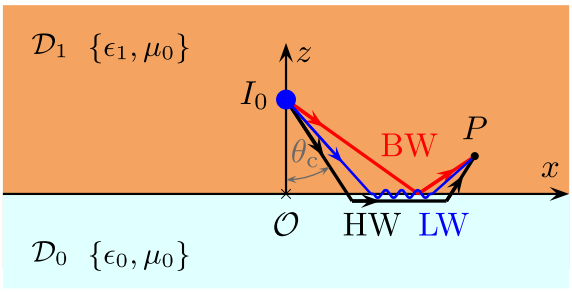

Fig. 3. Ray trajectories of the HW, LW, and BW constituents.

we encounter a simple pole singularity at $p = v^{-1}$ that for the chosen parameters, $c_1 < v < c_0$, lies on the branch cut emanating from $p = c_0^{-1}$. Consequently, by virtue of Cauchy's theorem and Jordan's lemma, the integration contour is deformed into the CdH path that can be defined by

$$px + \gamma_1(p)(z+h) = \tau \quad \text{for } \{\tau \in \mathbb{R};\, \tau > 0\} \tag{8}$$

where τ has the meaning of the time parameter. The latter equation can be satisfied along a hyperbolic path, where the horizontal slowness parameter takes the values $p_B = p_B(\tau)$ and $p_B^* = p_B^*(\tau)$, and around a loop encircling the branch cut, where $p_H = p_H(\tau)$ and $p_H^* = p_H^*(\tau)$ in $\mathrm{Im}(p) \gtrless 0$, respectively (see Fig. 2).

In contrast to the more prevalent transform-domain method (see [10, Sec. 11.8]), the CdH approach allows to associate each singularity in the complex slowness plane with a *causal* physical phenomenon that occurs in the resulting wave motion. This can be illustrated via Fig. 2. Here, the integration along the straight segments $p_H \cup p_H^*$ can be associated with the HW contribution, whose arrival time can be linked to the branch point $p = 1/c_0$ via (8) as

$$T_H = |x|c_0^{-1} + (z+h)\big(c_1^{-2} - c_0^{-2}\big)^{1/2}. \tag{9}$$

Upon noting that the intersection of the hyperbolic BW path with $\mathrm{Im}(p) = 0$ is at $p_0 = (|x|/r)c_1^{-1}$, where $r = [x^2 + (z+h)^2]^{1/2}$, it can be concluded that the HW contribution shows up in the bounded region of space, where $p_0 > c_0^{-1}$, that is,

$$|x|/r > \sin(\theta^c) = c_1/c_0 \tag{10}$$

where we introduced the "critical angle" θ^c. The latter can be associated with the "total reflection" against the interface. A similar line of reasoning can be readily pursued to analyze the contribution of the pole singularity at $p = v^{-1}$ that is to be associated with the reflected Cherenkov effect. Indeed, upon carrying out the integration around the pole, it is found that

$$E_y^{r;C}(x,z,t) = \frac{-\mu_0 I_0}{2(v^2/c_1^2 - 1)^{1/2}} \frac{v^2/c_1^2 + v^2/c_0^2 - 2}{v^2/c_1^2 - v^2/c_0^2} \delta(t - T_C) \tag{11}$$

where T_C denotes the arrival time of the Cherenkov reflected wavefield constituent. This arrival time can be determined by using $p = v^{-1}$ in (8), which yields [see (9)]

$$T_C = xv^{-1} + (z+h)\big(c_1^{-2} - v^{-2}\big)^{1/2}. \tag{12}$$

In a similar fashion as the HW constituent, the Cherenkov reflected radiation occurs only in a bounded region of space, where [see (10)]

$$x/r > c_1/v. \tag{13}$$

Apparently, the HW and Cherenkov reflected-field constituents bear similarities. Finally, the BW wavefield follows upon carrying out the integration along the hyperbolic contour $p_B \cup p_B^*$. Its arrival time, say T_B, corresponds to the intersection point $p_0 = (|x|/r)c_1^{-1}$, which via (8) leads to

$$T_B = rc_1^{-1}. \tag{14}$$

The ray trajectories of both HW and BW field constituents are shown in Fig. 3. A closer inspection of (9), (12), and (14) reveals that for the given parameters, $c_1 < v < c_0$, we have $T_H < T_C < T_B$. The latter implies that the Cherenkov effect shows up between the occurrence of the HW and BW constituents.

B. Stationary Line Source

The reflected field due to a stationary electric-line source can be derived from (5), where we let $v = 0$, i.e.,

$$\hat{E}_y^r(x,z,s) = -\frac{\mu_0 I_0}{2i\pi} \int_{p=-i\infty}^{i\infty} \exp\{-s[px + \gamma_1(p)(z+h)]\} \times \tilde{R}_\perp(p) \frac{dp}{2\gamma_1(p)}. \tag{15}$$

Likewise the integrand in (5), the integrand in (15) has algebraic branch points at $p = \pm c_{0,1}^{-1}$ [see (7)]. But, since the denominator of the transform-domain reflection coefficient [see (6)], i.e.,

$$\Delta_\perp(p) = \gamma_1(p)/\mu_0 + \gamma_0(p)/\mu_0 \tag{16}$$

never vanishes in the entire complex p-plane, the integrand, in contrast to the transform-domain expression corresponding to the traveling line source, has no pole in the complex p-plane (see Fig. 4). Consequently, neither true surface waves (see [24], for example) nor Cherenkov waves can be excited in this (static-source) case.

It will be shown, however, that the absence of a pole singularity in the complex p-plane does not necessarily exclude the existence of an interesting TD wave feature that occurs between the HW and BW constituents. For that reason, we shall more closely evaluate the contribution along the HW CdH path, $p_H \cup p_H^*$. Accordingly, upon combining the

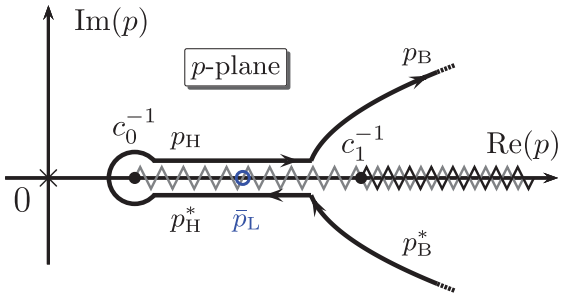

Fig. 4. CdH path in the complex p-plane pertaining to the reflected field above the half-space due to the *stationary* line source for $x > 0$. The gray and black zigzags represent the branch cuts originating at c_0^{-1} and c_1^{-1}, respectively.

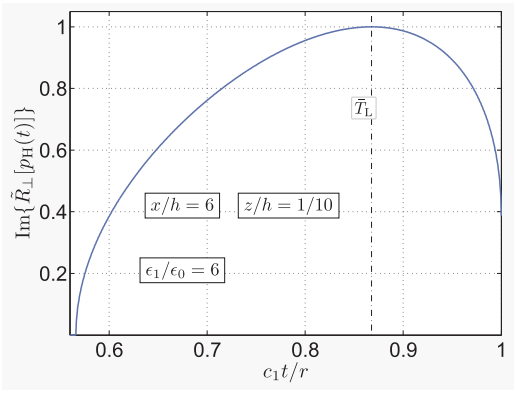

Fig. 5. Imaginary part of the reflection coefficient along the CdH-HW path.

contributions from p_H and p_H^*, the HW contribution follows as:

$$E_y^{r;H}(x,z,t) = -(\mu_0 I_0/2\pi)\mathrm{Im}\{\tilde{R}_\perp[p_H(t)]\} \times \frac{H(t-T_H)-H(t-T_B)}{(T_B^2-t^2)^{1/2}}. \quad (17)$$

Apart from the factor with the typical inverse square-root singularity at the arrival time of BW [14, eq. (3.4.13)], the amplitude of the HW constituent depends on the (imaginary value of the) reflection coefficient along $p_H(t)$ in $T_H < t < T_B$. Along this CdH-HW path, γ_0 is purely imaginary, while γ_1 is real-valued and positive, i.e.,

$$\gamma_0(p_H) = -\mathrm{i}\left(p_H^2 - c_0^{-2}\right)^{1/2} \text{ and } \gamma_1(p_H) = \left(c_1^{-2} - p_H^2\right)^{1/2}. \quad (18)$$

The amplitude of the HW constituent can be then specified more explicitly via

$$\mathrm{Im}\left[\tilde{R}_\perp(p_H)\right] = \frac{2\left(c_1^{-2}-p_H^2\right)^{1/2}\left(p_H^2-c_0^{-2}\right)^{1/2}}{c_1^{-2}-c_0^{-2}} \quad (19)$$

which is a relatively simple function of p_H. Consequently, it is straightforward to show that this function attains its maximum $(=1)$ at $p_H = \bar{p}_L$, where

$$\left(c_1^{-2}-\bar{p}_L^2\right)^{1/2} - \left(\bar{p}_L^2 - c_0^{-2}\right)^{1/2} = 0. \quad (20)$$

It is noted that this equation bears a resemblance with $\Delta_\perp(p) = 0$ evaluated along the CdH-HW path. Indeed, using (18) in (16), it is found that $\Delta_\perp(p_H) = 0$ is equivalent to

$$\left(c_1^{-2}-p_H^2\right)^{1/2} - \mathrm{i}\left(p_H^2 - c_0^{-2}\right)^{1/2} = 0. \quad (21)$$

Accordingly, it is seen that the condition for the existence of causal surface waves, $\Delta_\perp(p) = 0$, is in the interval $T_H < t < T_B$ identical to the condition for existence of a maximum of the HW amplitude, if the vertical slowness γ_0 is replaced with Γ_0 according to

$$\gamma_0 = -\mathrm{i}\left(p^2 - c_0^{-2}\right)^{1/2} \Rightarrow \Gamma_0 = -\left(p^2 - c_0^{-2}\right)^{1/2}. \quad (22)$$

Interestingly, under this replacement, the transform-domain field as *transmitted* to $\mathcal{D}_0$ has the following form:

$$\tilde{E}_y^t(p,z,s) \Rightarrow -(\mu_0 I_0/2s\gamma_1)(1+\tilde{R}_E) \times \exp(-s\gamma_1 h)\exp\left[-s\left(p^2-c_0^{-2}\right)^{1/2} z\right] \quad (23)$$

which in the lower half-space, where $z < 0$, represents a function that grows exponentially with the increasing distance away from the interface. That is a typical property associated with LW phenomena [2]. While the surface-wave condition (21) can hardly ever be satisfied, (20) leads to

$$\bar{p}_L = \pm\left(c_0^{-2} + c_1^{-2}\right)^{1/2}/\sqrt{2} \quad (24)$$

thereby localizing a local maximum in the amplitude of HW along the CdH-HW path (see Fig. 4). Consequently, the use of (24) in (8) yields the corresponding "arrival time" [see (9)]

$$\bar{T}_L = \frac{|x|}{\sqrt{2}}\left(c_1^{-2}+c_0^{-2}\right)^{1/2} + \frac{z+h}{\sqrt{2}}\left(c_1^{-2}-c_0^{-2}\right)^{1/2}. \quad (25)$$

Fig. 5 illustrates a typical behavior of (the imaginary value of) the reflection coefficient along the CdH-HW path. For the chosen parameters, i.e., $\epsilon_1/\epsilon_0 = 6$, $x = 6h$ and $z = h/10$, the HW arrives at the field point at $T_H/T_B \simeq 0.57$ and the coefficient takes the maximum value $(=1)$ at $\bar{T}_L/T_B \simeq 0.87$.

Since there is no disturbance wavefront associated with $\bar{p}_L$ and $\bar{T}_L$, the corresponding feature is, strictly mathematically speaking, a (*pseudo*)-LW (see [18], for another example from this category, and the Appendix). Since $c_0^{-1} < |\bar{p}_L| < c_1^{-1}$ for $c_0 > c_1$, the LW phenomenon occurs in between the HW's and BW's arrival, i.e., $T_H < \bar{T}_L < T_B$. Furthermore, in like manner as the HW and Cherenkov effect, the occurrence of LW is limited to a bounded region of space. Indeed, the LW shows up only if $\bar{p}_L < p_0$, which leads to [see (10)]

$$|x|/r > \sin\left(\vartheta_L^c\right) = c_1/\bar{v} = \left(1 + c_1^2/c_0^2\right)^{1/2}/\sqrt{2} \quad (26)$$

where ϑ_L^c denotes the corresponding LW "critical angle" and $\bar{v} = 1/|\bar{p}_L|$ is the "pseudo-wave speed" at which the LW "propagates" *along the interface*. The corresponding LW ray trajectory is shown in Fig. 3, where the (horizontal) section that is traversed at the speed $\bar{v}$ is denoted by a wavy line.

On account of the relation, $c_0^{-1} < |\bar{p}_L| < c_1^{-1}$ for $c_0 > c_1$, it is seen that the condition for the existence of the HW [see (10)] is always satisfied if the LW condition (26) holds true, i.e., $\vartheta_L^c > \theta^c$. In other words, for a given contrast ratio, c_0/c_1, and for a fixed vertical propagation path, $z+h$, the LW occurs at a larger horizontal offset $|x|$ compared to the one pertaining to HW. From (24) and (26) [see also (9) and (25)], we may

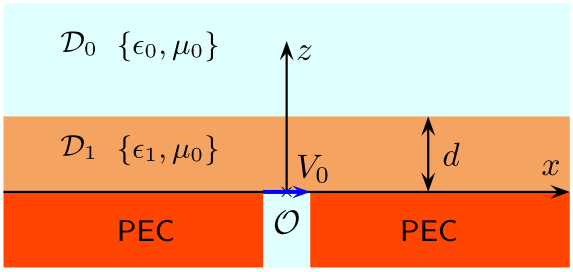

Fig. 6. Slot-excited dielectric slab.

express the speed of LW, $\bar{v}$, in the following form:

$$\bar{v} = \sqrt{2}/\left(c_0^{-2} + c_1^{-2}\right)^{1/2}. \tag{27}$$

We note that this speed corresponds to the "average permittivity" pertaining to half-spaces $\mathcal{D}_0$ and $\mathcal{D}_1$. Indeed, if we define the relative permittivity, $\epsilon_r > 1$, via $\sqrt{\epsilon_r} = c_0/c_1$, then (27) implies that $c_0^2/\bar{v}^2 = (\epsilon_r + 1)/2$.

A similar quantitative analysis can be applied to more complex problem configurations. This is illustrated in Sections IV and V.

IV. Slot-Excited Dielectric Slab

A detailed CdH analysis of the pulsed EM radiation from the slot antenna under consideration can be found in [25] (see also [26] for a more general slot antenna configuration). Since the corresponding TD LW analysis (see Section IV-B) relies in part on the results of [25], its main outcomes are next, for the reader's convenience, briefly summarized.

The antenna configuration (see Fig. 6) consists of a slot of vanishing width in a PEC wall that, except for the slot, occupies the $z < 0$ half-space. The slot is infinitely long and is cut along the y-axis. The slotted PEC screen is covered by a dielectric slab that occupies domain $\mathcal{D}_1 = \{-\infty < x < \infty, -\infty < y < \infty, 0 < z < d\}$, where $d > 0$ denotes its thickness. The slot antenna radiates into an unbounded domain $\mathcal{D}_0 = \{-\infty < x < \infty, -\infty < y < \infty, d < z < \infty\}$. As far as the EM constitutive properties are concerned, the media in $\mathcal{D}_0$ and $\mathcal{D}_1$ are again described by (real-valued and positive) scalar parameters $\{\epsilon_0, \mu_0\}$ and $\{\epsilon_1, \mu_0\}$, respectively.

The antenna is excited at $t = 0$ via its narrow slot, along which the (y-independent) excitation electric-field distribution is described by

$$E_x(x, 0^+, t) = V_0\delta(x)\mathrm{H}(t) \text{ for all } x \in \mathbb{R} \text{ and } t > 0 \tag{28}$$

where V_0 (in V) denotes the excitation voltage amplitude. Since the problem configuration as well as its excitation are y-independent, only the (H-polarized) EM field components, $\{H_y, E_x, E_z\}(x, z, t)$, are excited. Across the planar interface in between $\mathcal{D}_0$ and $\mathcal{D}_1$, the tangential EM field components satisfy the continuity-type conditions

$$\lim_{z\downarrow d}\{E_x, H_y\}(x, z, t) = \lim_{z\uparrow d}\{E_x, H_y\}(x, z, t) \quad \text{for all } x \in \mathbb{R} \text{ and } t > 0. \tag{29}$$

It is the goal of Sections IV-A–IV-C to study the TD radiated EM fields satisfying the corresponding EM field equations under the excitation and continuity conditions (28) and (29), respectively.

A. Time-Domain Solution

To solve the thus formulated antenna radiation problem, we may pursue the CdH approach presented in [25]. To that end, we combine the time Laplace transform (1) with the wave-slowness representation in the x-direction (2), again. Using the integral transformations, the magnetic field strength as observed in $\mathcal{D}_0$ can be in the s-domain expressed as (see [25, eq. (19)])

$$\hat{H}_y(x, z, s) = \frac{\epsilon_1 V_0}{2\pi\mathrm{i}}\int_{p=-\mathrm{i}\infty}^{\mathrm{i}\infty} \exp(-spx) \times \frac{\tilde{T}_\parallel(p)\exp\{-s[\gamma_1 d + \gamma_0(z-d)]\}}{1 - \tilde{R}_\parallel(p)\exp(-2s\gamma_1 d)}\frac{\mathrm{d}p}{\gamma_1} \tag{30}$$

where the (transform-domain) transmission and reflection coefficients are given by

$$\tilde{T}_\parallel(p) = 1 + \tilde{R}_\parallel(p) = \frac{2\gamma_1/\epsilon_1}{\gamma_1/\epsilon_1 + \gamma_0/\epsilon_0} \tag{31}$$

in which $\gamma_{0,1}(p)$ are defined via (7). As far as its analytical properties in the complex p-plane are concerned, it is seen that the integrand in (30) has only branch-point singularities due to γ_0 that are associated with the branch cut along $\{c_0^{-1} < |\mathrm{Re}(p)| < \infty, \mathrm{Im}(p) = 0\}$. In contrast to the standard real-FD representation (see [10, Sec. 11.8], for example), the integrand under the conditions laid upon the Laplace-transform parameter s and $\gamma_{0,1}$ does not have any poles in the entire complex p-plane. This, in turn, implies again the absence of true surface waves.

To perform the exact transformation of (30) back to the TD, the integrand is expanded as

$$\hat{H}_y(x, z, s) = \sum_{n=0}^{\infty}\hat{H}_y^{[n]}(x, z, s) \tag{32}$$

where its nth generalized-ray constituent has the form that is amenable to the CdH technique, i.e.,

$$\hat{H}_y^{[n]}(x, z, s) = \frac{\epsilon_1 V_0}{2\pi\mathrm{i}}\int_{p=-\mathrm{i}\infty}^{\mathrm{i}\infty} \tilde{T}_\parallel(p)\tilde{R}_\parallel^n(p) \times \exp\{-s[px + \gamma_1 z_n + \gamma_0(z-d)]\}\mathrm{d}p/\gamma_1 \tag{33}$$

for $z \geq d$, where $z_n = (2n+1)d$. Note that in contrast to (30), the integrand in (33) is made single valued by introducing the horizontal branch cuts along $\mathrm{Im}(p) = 0$ as indicated before in Fig. 4 for $x > 0$.

For our purposes, it is next sufficient to provide the TD original of (33) for field points lying just at the interface at $z = d$. Hence, following the joint-inversion strategy presented in [25, Appendix A], the TD counterpart of (33) follows as:

$$H_y^{[n]}(x, d, t) = H_y^{\mathrm{H};[n]}(x, d, t) + H_y^{\mathrm{B};[n]}(x, d, t) \tag{34}$$

where the nth HW and BW constituents can be expressed as [see (17)]

$$H_y^{\mathrm{H};[n]}(x,d,t) = (\epsilon_1 V_0/\pi)\,\mathrm{Im}\{\tilde{T}_\parallel[p_\mathrm{H}(t)]\tilde{R}_\parallel^n[p_\mathrm{H}(t)]\} \times \frac{\mathrm{H}(t-T_{\mathrm{H};n})-\mathrm{H}(t-T_{\mathrm{B};n})}{(T_{\mathrm{B};n}^2-t^2)^{1/2}} \quad (35)$$

and

$$H_y^{\mathrm{B};[n]}(x,d,t) = (\epsilon_1 V_0/\pi)\,\mathrm{Re}\{\tilde{T}_\parallel[p_\mathrm{B}(t)]\tilde{R}_\parallel^n[p_\mathrm{B}(t)]\} \times \frac{\mathrm{H}(t-T_{\mathrm{B};n})}{(t^2-T_{\mathrm{B};n}^2)^{1/2}} \quad (36)$$

respectively. Again, the HW constituent, in like manner as an LW, shows up only in the subregion of space bounded by the condition [see (10)]

$$|x|/r_n > \sin(\theta^\mathrm{c}) = c_1/c_0 \quad (37)$$

thereby introducing again the "critical angle" θ^c. In (35) and (36), we used $T_{\mathrm{B};n}$ and $T_{\mathrm{H};n}$ to denote the arrival times of the nth BW and HW constituent, respectively. Through their expressions, i.e.,

$$T_{\mathrm{B};n} = r_n c_1^{-1}, \quad (38)$$

$$T_{\mathrm{H};n} = |x|c_0^{-1} + z_n(c_1^{-2}-c_0^{-2})^{1/2} \quad (39)$$

with $r_n = (x^2+z_n^2)^{1/2} > 0$, one may construct the corresponding ray trajectories. Fig. 7 shows examples of the HW- and BW-ray trajectories pertaining to the zeroth and first constituents. For the sake of completeness, in the TD expressions we used the values of the (time-dependent) slowness parameter p along the BW and HW CdH paths in $\mathrm{Im}(p) > 0$, viz,

$$p_\mathrm{B}(t) = (x/r_n^2)t + \mathrm{i}(z_n/r_n^2)(t^2-T_{\mathrm{B};n}^2)^{1/2} \quad (40)$$

for all $t > T_{\mathrm{B};n}$, and

$$p_\mathrm{H}(t) = (x/r_n^2)t - (z_n/r_n^2)(T_{\mathrm{B};n}^2-t^2)^{1/2} + \mathrm{i}0 \quad (41)$$

for $T_{\mathrm{H};n} < t < T_{\mathrm{B};n}$. It is clear from (35), (36), (38), and (39) that the $(n+1)$th wave constituent arrives at the field point later than the nth one. Consequently, the total number of generalized-ray constituents is finite in any bounded time window of observation.

B. Time-Domain Leaky-Wave Analysis

We shall next assume that the horizontal offset between the slot and the field point at (x,d) is large enough such that condition (37) for the existence of HWs is for a given contrast ratio, say c_0/c_1, satisfied. For the sake of brevity, we shall further express the latter via the relative permittivity of the slab, $\sqrt{\epsilon_\mathrm{r}} = c_0/c_1$. Consequently, following the lines of reasoning pursued in Section III-B, we may study the condition under which the pulse shape of an HW constituent (35) exhibits a local maximum. For the sake of clarity, the corresponding analysis is first carried out for the zeroth constituent (i.e., $n = 0$), the amplitude of which is proportional to $\mathrm{Im}[\tilde{T}_\mathrm{H}(p_\mathrm{H})]$ for $c_0^{-1} < |p_\mathrm{H}| < p_0$, where $p_0 = c_1^{-1}(|x|/r_n)$ denotes the intersection of the CdH-BW path with

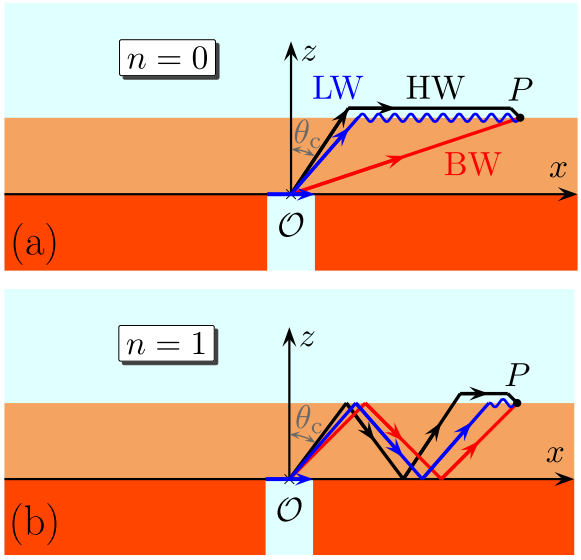

Fig. 7. Ray trajectories of the nth HW, LW and BW constituents. (a) $n = 0$. (b) $n = 1$.

$\mathrm{Im}(p) = 0$ [see (40)]. With reference to the chosen branch cuts (see Fig. 4), it is seen that

$$\mathrm{Im}[\tilde{T}_\parallel(p_\mathrm{H})] = \frac{2\epsilon_\mathrm{r}}{\epsilon_\mathrm{r}^2-1}\frac{(c_1^{-2}-p_\mathrm{H}^2)^{1/2}(p_\mathrm{H}^2-c_0^{-2})^{1/2}}{p_\mathrm{H}^2-c_1^{-2}/(\epsilon_\mathrm{r}+1)} \quad (42)$$

along the HW part of the CdH contour. Upon solving $\partial_p \mathrm{Im}[\tilde{T}_\parallel(p)] = 0$ for $c_0^{-1} < |p| < p_0$, it is straightforward to demonstrate that the HW amplitude takes its maximum value at [see (24)]

$$\bar{p}_{\mathrm{L};0} = \pm\frac{1}{c_1}\left(\frac{\epsilon_\mathrm{r}+1}{\epsilon_\mathrm{r}^2+1}\right)^{1/2}. \quad (43)$$

First, it is easy to show that $c_0^{-1} < |\bar{p}_{\mathrm{L};0}| < c_1^{-1}$ for any bounded $\epsilon_\mathrm{r} > 1$. Second, to reach the maximum along the CdH-HW path, the condition $|\bar{p}_{\mathrm{L};0}| < p_0$ must be met. This condition can be rewritten as [see (37)]

$$|x|/r_0 > \sin(\vartheta_\mathrm{L}^\mathrm{c}) = c_1/\tilde{v} = \left(\frac{\epsilon_\mathrm{r}+1}{\epsilon_\mathrm{r}^2+1}\right)^{1/2} \quad (44)$$

which clearly bounds the region of space where the zeroth-order LW effect shows up and we used $\tilde{v} = 1/|\bar{p}_{\mathrm{L};0}|$. Since $\vartheta_\mathrm{L}^\mathrm{c} > \theta^\mathrm{c}$ for $\epsilon_\mathrm{r} > 1$, the occurrence of the "bump" in the HW constituent of the received signal thus requires, for a given dielectric slab, a larger horizontal offset than the one needed for the excitation of the HW [see (37)]. Finally, the "arrival time" of this zeroth-order LW effect follows from $\bar{T}_{\mathrm{L};0} = \bar{p}_{\mathrm{L};0}x + \gamma_1(\bar{p}_{\mathrm{L};0})d$ as [see (39) for $n = 0$]:

$$\bar{T}_{\mathrm{L};0} = \frac{|x|}{c_1}\left(\frac{\epsilon_\mathrm{r}+1}{\epsilon_\mathrm{r}^2+1}\right)^{1/2} + \frac{d}{c_1}\left(\frac{\epsilon_\mathrm{r}^2-\epsilon_\mathrm{r}}{\epsilon_\mathrm{r}^2+1}\right)^{1/2}. \quad (45)$$

Despite its apparent complexity, (45) has a straightforward geometric interpretation. Indeed, $\bar{T}_{\mathrm{L};0}$ can be explained through the LW ray trajectory shown in Fig. 7(a). This graphical representation can be clarified by writing $\bar{T}_{\mathrm{L};0} = |x|/\tilde{v} + (d/c_1)\cos(\vartheta_\mathrm{L}^\mathrm{c})$, where $\vartheta_\mathrm{L}^\mathrm{c}$ is associated with the corresponding LW "critical angle" and $\tilde{v}$ with the speed at which the LW

effect travels along the interface [see (44)]. In contrast to $\bar{v}$ given by (27), the actual $\tilde{v}$ cannot be directly related to the "average permittivity" of the adjoining media, but $c_0^2/\tilde{v}^2 = \epsilon_r(\epsilon_r+1)/(\epsilon_r^2+1)$ instead.

Adopting the approach pursued in Section III-B, it is next briefly demonstrated that these results can also be obtained using the replacement (22). Indeed, it is first observed using (33) with $n=0$ that a true surface wave would be excited, if the transmission coefficient [see (31)] had a pole in the complex p-plane, that is, if [see (16)]

$$\Delta_{\parallel}(p) = \gamma_1(p)/\epsilon_1 + \gamma_0(p)/\epsilon_0 = 0. \tag{46}$$

Since the real part of the square roots is kept positive throughout the complex p-plane, (46) cannot hold true in the cut p-plane. But, if the vertical slowness corresponding to $\mathcal{D}_0$, γ_0 is replaced by Γ_0 according to (22), then we get an alternative equation, say $\bar{\Delta}_{\parallel}(p)=0$. The latter equation can be solved for $p=\bar{p}_{\mathrm{L};0}$, at which the amplitude of the HW constituent attains its maximum [see (43)]. Under the replacement (22), the propagation factor corresponding to $\mathcal{D}_0$ takes the following form [see (33)]:

$$\exp\big[-s\gamma_0(z-d)\big] \Rightarrow \exp\Big[s\big(p^2-c_0^{-2}\big)^{1/2}(z-d)\Big]. \tag{47}$$

Apparently, (47) for $s>0$ and the positive square root represents an exponentially increasing function as the field point is moving away from the interface in $z>d$.

Finally, it is noted that the higher-order wave constituents (as well as other problem configurations) can be analyzed along the same lines. Indeed, taking $n=1$ in (35), for example, it is found that the HW amplitude $\mathrm{Im}[\tilde{T}_{\parallel}(p_{\mathrm{H}})\tilde{R}_{\parallel}(p_{\mathrm{H}})]$ takes its maximum at [see (43)]

$$\bar{p}_{\mathrm{L};1} = \pm\frac{1}{c_1}\left[\frac{\epsilon_r^3+(6-\sqrt{33})\epsilon_r^2+(6+\sqrt{33})\epsilon_r+3}{\epsilon_r^4+12\epsilon_r^2+3}\right]^{1/2} \tag{48}$$

while the corresponding LW "arrival time" follows from:

$$\bar{T}_{\mathrm{L};1} = \bar{p}_{\mathrm{L};1}x + \gamma_1(\bar{p}_{\mathrm{L};1})z_1. \tag{49}$$

Fig. 7(b) shows the corresponding LW ray trajectory. The presented results are further illustrated in Section IV-C through numerical examples.

C. Illustrative Examples

We next illustrate the results presented in Sections IV-A and IV-B on selected examples. To that end, we shall calculate the unit-step-excited (i.e., $V_0 = 1\,\mathrm{V}$) magnetic-field on the surface $z=d$ of a dielectric slab of thickness $d = 1.0\,\mathrm{mm}$. The TD responses are evaluated via (34) and (35) and the TD counterpart of (32) in the bounded time window $0 \le c_1 t/d \le 6$.

In the first example, the horizontal offset of the field point is $x = 4\,d$ and the dielectric constant of the slab is $\epsilon_r = 4$. Fig. 8(a) shows the corresponding magnetic-field waveform along with the arrival times of all HWs, BWs and pLWs that showed up in the chosen time window. First, at $c_1 T_{\mathrm{H};0}/d \simeq 2.87$ the zeroth HW arrives at the field point.

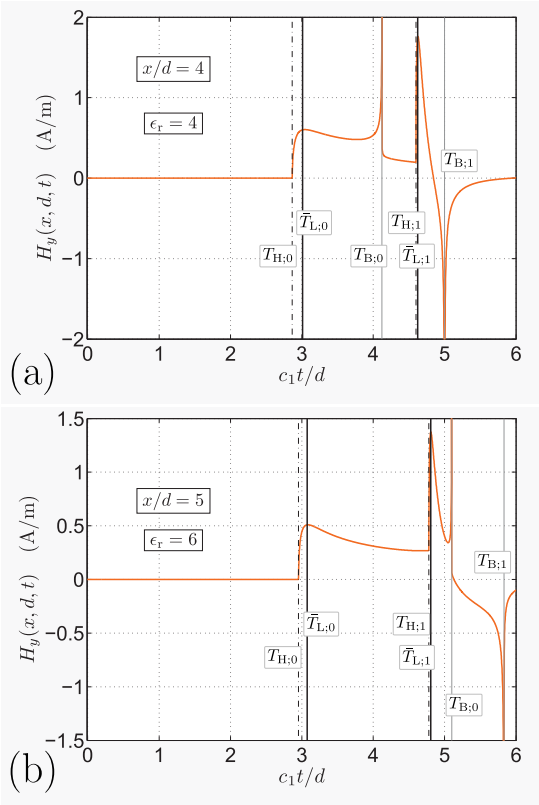

Fig. 8. Unit-step-excited magnetic-field strength at (a) $(x,z)=(4d,d)$ for $\epsilon_r=4$ and (b) $(x,z)=(5d,d)$ for $\epsilon_r=6$.

Shortly after this arrival, the signal takes its local maximum at $c_1\bar{T}_{\mathrm{L};0}/d \simeq 3.01$. The next signal discontinuity at $c_1 T_{\mathrm{B};0}/d \simeq 4.12$ is associated with the occurrence of the zeroth BW, where the signal exhibits the typical line-source inverse square-root singularity [see (36)]. The following sharp peak occurs at $c_1\bar{T}_{\mathrm{L};1}/d \simeq 4.62$ almost immediately after the arrival time of the first-order HW at $c_1 T_{\mathrm{H};1}/d \simeq 4.60$. It is clearly seen that the temporal separation of both first-order LW and BW from the corresponding HW is significantly smaller compared to the zeroth wave constituents.

A somewhat different waveform is shown in Fig. 8(b) for $x = 5\,d$ and $\epsilon_r = 6$. Here, owing to the relatively high permittivity of the slab, the temporal separation between HWs and pLWs is smaller with respect to the previous example [see (39) and (45)]. In addition, it is seen now that the zeroth BW (with its inverse square-root behavior) reaches the field point at $c_1 T_{\mathrm{B};0}/d \simeq 5.10$ later than both zeroth and first HWs and pLWs with their arrival times at $c_1 T_{\mathrm{H};0}/d \simeq 2.95$, $c_1\bar{T}_{\mathrm{L};0}/d \simeq 3.08$ and $c_1 T_{\mathrm{H};1}/d \simeq 4.78$, $c_1\bar{T}_{\mathrm{L};1}/d \simeq 4.81$, respectively. Finally, the first BW shows up at $c_1 T_{\mathrm{B};1}/d \simeq 5.83$.

V. Electric-Current Excited Infinite Slot

In this section, we shall briefly study the EM waves excited along an infinite slot in a PEC screen that separates two homogeneous media. This problem has been analyzed before in the FD with regard to the excitation of LWs [6].

The analyzed problem configuration consists of a narrow infinite slot that occupies domain $\mathcal{S} = \{-w/2 < x < w/2,$

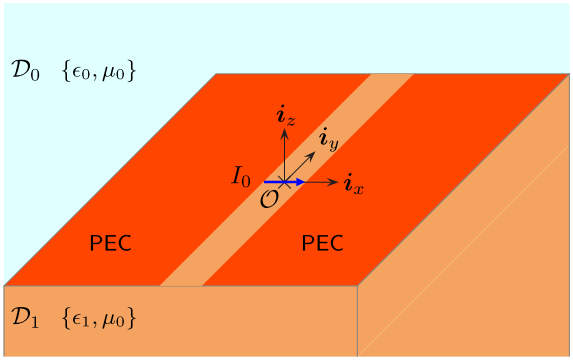

Fig. 9. Electric-current-excited slot at the interface of two half-spaces.

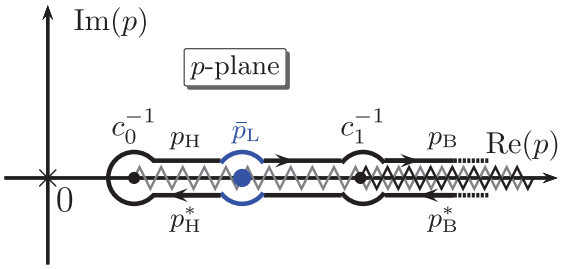

Fig. 10. CdH path in the complex p-plane pertaining to the voltage excited along the slot for $y > 0$. The gray and black zigzags represent the branch cuts originating at c_0^{-1} and c_1^{-1}, respectively.

$-\infty < y < \infty, z = 0\}$, where $w > 0$ denotes its (relatively small) width. The PEC screen is located at the interface between two homogeneous half-spaces, $\mathcal{D}_0 = \{-\infty < x < \infty, -\infty < y < \infty, z < 0\}$ and $\mathcal{D}_1 = \{-\infty < x < \infty, -\infty < y < \infty, z > 0\}$ (see Fig. 9). Their EM properties are described by scalar parameters $\{\epsilon_{0,1}, \mu_0\}$, again, thus implying the wavespeeds $c_{0,1} = (\mu_0\epsilon_{0,1})^{-1/2}$, respectively. Following the excitation model introduced by Galejs [27], the slot is excited by a lumped electric-current source that can be defined via its electric-current surface density [see (3)]:

$$\partial J_x(x, y, t) = I_0 \Pi_w(x)\delta(y)\mathrm{H}(t) \tag{50}$$

where I_0 (in A) represents the electric-current amplitude, again, and $\Pi_w(x)$ denotes the rectangular function of width w, i.e., $\Pi_w(x) = 1$ if $x \in [-w/2, w/2]$ and $\Pi_w(x) = 0$ elsewhere. Our analysis aims at (the space-time distribution of) the voltage induced across the narrow slot, say $V = V(y, t)$.

The thus defined problem can be formulated via the TD EM reciprocity theorem of the time-convolution type [28, Sec. 28.2]. This theorem can be used to link the actual *scattered* EM-field, defined with respect to the "short-circuited slot" and further denoted by superscript $^{\mathrm{s}}$, with the *auxiliary* testing EM-field (to be denoted by superscript $^{\mathrm{T}}$). Upon applying the theorem to both $\mathcal{D}_0$ and $\mathcal{D}_1$, we get two relations whose difference leads to (see [29, eq. (3)])

$$\int_{\mathcal{S}} \partial K_y^{\mathrm{s}}(x, y, t) *_t \left[H_y^{\mathrm{T}}(x, y, 0^+, t) - H_y^{\mathrm{T}}(x, y, 0^-, t)\right]\mathrm{d}A = -\int_{\mathcal{S}} \partial J_x(x, y, t) *_t \partial K_y^{\mathrm{T}}(x, y, t)\mathrm{d}A \tag{51}$$

where the induced magnetic-current surface density, $K_y^{\mathrm{s}}(x, y, t)$, can be related to the desired voltage as

$$\partial K_y^{\mathrm{s}}(x, y, t) \simeq \frac{2}{\pi w} \frac{\Pi_w(x)}{[1 - (2x/w)^2]^{1/2}} V(y, t). \tag{52}$$

Through (52) we postulate the typical inverse-square root singularity of the axial magnetic current along the edges of the slot. The way how the testing-current density, $K_y^{\mathrm{T}}(x, y, t)$, is related to the testing fields $H_y^{\mathrm{T}}(x, y, z, t)$ in $\mathcal{D}_{0,1}$ can be easily determined in the transform domain. To that end, we next employ the Laplace transform (1) with the wave slowness representation of the type defined via (2) in both x- and y-directions. This joint-transform CdH approach enables to cast the TD reciprocity relation (51) into the form of complex-slowness integrals (see [30, Sec. 14.2], for example). In the next step, following the lines of reasoning presented in [6], the integration pertaining to the transverse direction is carried out analytically using [31, Formula 11.4.48] and from the thus obtained relation we readily derive the transform-domain induced voltage, say $\tilde{V}(p, s)$. Then, using the slowness representation of the type (2), we may write

$$\hat{V}(y, s) = \frac{s\mu_0 I_0 \pi}{2\mathrm{i}\pi} \int_{p=-\mathrm{i}\infty}^{\mathrm{i}\infty} \frac{\exp(-spy)}{\Delta(p, s)}\mathrm{d}p \tag{53}$$

where p has the meaning of the axial slowness along the y-direction, and

$$\Delta(p, s) = s^2\gamma_0^2(p)\mathrm{I}_0[s\gamma_0(p)a]\mathrm{K}_0[s\gamma_0(p)a] + s^2\gamma_1^2(p)\mathrm{I}_0[s\gamma_1(p)a]\mathrm{K}_0[s\gamma_1(p)a] \tag{54}$$

in which $\mathrm{I}_0(x)$ and $\mathrm{K}_0(x)$ denote the modified Bessel functions of the first and second kind, respectively, and we have introduced the "equivalent radius" $a = w/4$, for brevity. Owing to the definition of square roots via (7), the horizontal branch cuts in the complex p-plane along $\{c_{0,1}^{-1} \le |\mathrm{Re}(p)| < \infty, \mathrm{Im}(p) = 0\}$ are introduced, again. Since the integrand meets the condition for the applicability of Jordan's lemma [28, p. 1054], the original contour can be replaced with the loop along the branch cuts. In the process of deformation, potential pole contributions must be accounted for. Accordingly, upon closer inspection using the small-argument expansions of the Bessel functions [31, Formulas 9.6.7 and 9.6.8], (54) reveals that for a vanishing slot's width we may write $\Delta(p, s) \simeq s^2[\gamma_0^2(p) + \gamma_1^2(p)]\mathrm{K}_0[s\gamma_0(p)a]$. Under this approximation, the equation $\Delta(p, s) = 0$ is satisfied at $p = \bar{p}_{\mathrm{L}}$ as given by (24), again. Using $\bar{v} = 1/|\bar{p}_{\mathrm{L}}|$, it is seen that the contribution of the pole singularity, likewise the line-source excited LW effect along the half-space interface [see (27)], travels at the speed corresponding to the "average permittivity" (see [27, eq. (1)]).

Fig. 10 shows the corresponding complex p-plane for $y > 0$ with the CdH path encircling the branch cuts. The integration CdH contour consists of the CdH-BW and CdH-HW parts and of circular arcs of vanishing radius enclosing the branch-point and pole singularities at $p = c_{0,1}^{-1}$ and $p = \bar{p}_{\mathrm{L}}$, respectively. As far as the singularities in the complex slowness plane are concerned, the transform-domain expression for the lumped-source-induced voltage in the narrow slot resembles the EM-field radiated from a traveling source

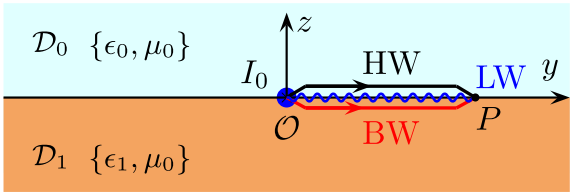

Fig. 11. Ray trajectories of the HW, LW, and BW constituents around the interface. The LW trajectory is represented by the blue wavy line.

(see Fig. 2). The singular points can be again associated with the arrival times of (causal) wave constituents forming the total wave motion. Indeed, the distance from the electric-current source [see Fig. 9 and (50)] to the field point at $(0, y, 0)$ is first traversed by the HW constituent at slowness $p = c_0^{-1}$. In a similar fashion, the LW and HW constituents travel at the slowness $p = \bar{v}^{-1}$ and $p = c_1^{-1}$, respectively. Accordingly, the HW, LW, and BW arrival times are given by

$$T_{\mathrm{H}} = |y|c_0^{-1} < \bar{T}_{\mathrm{L}} = |y|\bar{v}^{-1} < T_{\mathrm{B}} = |y|c_1^{-1} \tag{55}$$

respectively. The corresponding ray trajectories are indicated in Fig. 11.

Apparently, the LW feature shows up, again, between the arrival of HW and BW constituents. In contrast to the LW phenomena that were associated with the local maximum in the wave amplitude (see Sections III-B and IV-B), the LW described in this section can vaguely be explained as a traveling-source wave effect (see Section III-A). The study in this section is an initial step toward the examination of the field radiating *away* from the slot, this task being pivotal to elucidating the TD operation of a multitude of readily available LW antennas. A fully analytical treatment of the entailed 3-D EM problem seems (at least at this moment) not possible and, thus, it calls upon purely numerical strategies for its solution. This investigation is then deferred to future research.

VI. Discussion

LW antennas are currently studied and designed exclusively in the FD that requires an established steady state of time-harmonic EM fields. However, the tendency is now toward sophisticated, very complex modulations that squeeze the interval over which the true steady state can be actually assumed. To address the limitation, our study proposes a TD interpretation of LW phenomena along with an efficient analytical instrument to describe them in a *quantitative* manner. Accordingly, the results presented in this article can serve, for example, for understanding transient EM effects *at* the moment of interrupting the steady state and predicting the behavior of the LW antennas *during* the transition to the new steady state.

Although the present work is concerned with relatively simple problems only, the described CdH approach can be readily applied to localize the space-time LW propagation in significantly more complex problem configurations. This, in particular, applies to an N-layered structure, for which the corresponding CdH path can be constructed at once via straightforward iterative techniques [32, Ch. 2]. To our knowledge, such a general analytical methodology that is capable of

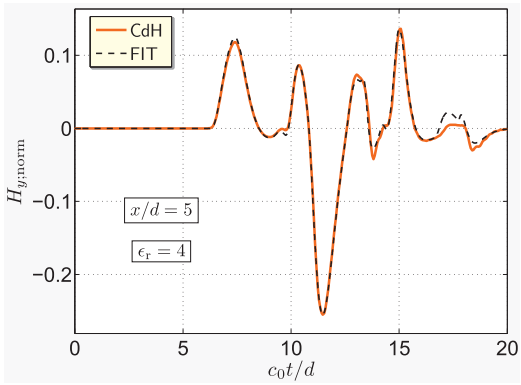

Fig. 12. Magnetic-field strength [normalized with respect to $(\epsilon_0/\mu_0)^{1/2} V_{\max}/w$] at $x/d = 5$ on the slot-excited dielectric slab of relative permittivity $\epsilon_{\mathrm{r}} = 4$ as calculated analytically using the CdH technique and numerically using the FIT.

quantifying TD EM LW effects is currently lacking in the literature on the subject.

The CdH technique is a well-established mathematical tool that yields analytical solutions in terms of expressions that can be evaluated with any prescribed accuracy. Consequently, this method is ideally suited for benchmarking (both in precision and speed) of purely numerical solutions. To gain confidence in our code implementations and to study complex problems that are not amenable to analytical solutions, we have also developed numerical models of the analyzed antennas [33], [34]. Fig. 12 shows the output of a typical validation test concerning the model of a slot-excited dielectric slab, the TD analysis of which was discussed in Section IV. The examined configuration is given in Fig. 6, that figure also explaining all notations employed in Fig. 12, except for $w > 0$ which is the slot's width. The slab between $z = 0$ and $z = d$ consists of a lossless dielectric with relative permittivity $\epsilon_{\mathrm{r}} = 4$. The represented quantity is the magnetic-field strength normalized by $(\epsilon_0/\mu_0)^{1/2} V_{\max}/w$ for a power-exponential shaped excitation $V_0(t)$, with amplitude $V_{\max}$ and raising power $\nu = 2$ [26, Appendix C]. The sampling point is located along the interface at $\{x, z\} = \{5d, d\}$. The plot in Fig. 12 cogently demonstrates the practical identity between our CdH analytical results and numerical ones calculated by means of the finite-integration technique (FIT), as implemented in CST Microwave Suite. Despite the fundamental differences in their mathematical formulation (see [33]), the results of simulations agree very well. For more details about the antenna models, the reader is referred to [33].

VII. Conclusion

In this work, LW phenomena have been analytically studied in the TD with the aid of the CdH joint-transform technique. For layered structures activated by a pulsed EM source, we have suggested that the TD LW effect can be associated with the local maximum that is in certain circumstances observed in the interval bounded by the HW and BW times of arrival. To enable the localization of such wave effects in space and time, the existence conditions, "arrival times" and their travel speeds have been discussed and analyzed *quantitatively*. Furthermore, it has been demonstrated that

the CdH transform-domain expression corresponding to the response of a localized-source-excited long slot in a conductive plane located on a dielectric half-space bears similarities with the one describing the reflected field induced by a point source traveling over the half-space. Consequently, we conclude that the analogy to Cherenkov's reflected wave can be instructive to grasp the physics of LW EM radiation from traveling-wave antennas.

APPENDIX
NOTES ON THE TERMINOLOGY

The term HW is frequently used in the seismological literature, where it is also known as the "*conical wave*" or "*lateral wave*" [35, Sec. 6.2]. In most of the EM literature the term "*lateral wave*" applies to the FD counterpart of the HW [36, Ch. 2], as in the FD analysis of acoustic waves in the neighborhood of an interface between two media.

A second type of wave employed in the text is the BW which travels with the wave speed in the relevant medium—in Fig. 3 it corresponds to the reflected wave. The terminology also originates from the seismological literature which is used to denote a wave constituent that travels via the interior of the Earth. Unlike the arrival of the BW, the HW arrival time is linearly related to the horizontal source-field spatial offset [see (9)]. Furthermore, while BW can exist at any location in space, HW occurs in a certain region of space only, which is determined by the critical angle of total internal reflection [see (10)]. In this sense, HW phenomena bear similarities with the *Cherenkov radiation*, which is a wave effect due to a uniformly moving EM source that passes through a medium at a higher speed with respect to the wave speed of that medium [19], [20]. Likewise, the TD HW can be associated with an equivalent *secondary* EM source traveling along the interface of two media, an exact space-time quantitative description of which is facilitated by the CdH method.

To conclude, this study highlighted the TD LW phenomenon. It should be noted that in line with the theory of hyperbolic partial differential equations [37, Sec. 5.8], if there is no wavefront associated with the observed wave effect, such a feature should be, strictly mathematically speaking, denoted as a "*pseudo-wave*" [18]. Accordingly, the wave speed (= the positive magnitude of velocity) term is then associated here with the speed of a disturbance front. A thorough discussion on the velocity of EM-field pulses can be found in [38].

Although the TD LW phenomenon may fall within the category of pseudo-waves, for precluding possible confusions, the employed terminology deliberately excluded the "pseudo" attribute. In like manner as HW, the TD LWs also occur in a bounded region of space determined by the corresponding critical angle. They too can be associated with equivalent secondary EM sources traveling along the intermedium interface with velocities exceeding the wave speed in the dielectric, thus bearing similarities with the Cherenkov radiation.

ACKNOWLEDGMENT

The research reported in this article was carried out during a research stay M. Štumpf had effectuated at the THz Sensing Group, TU Delft.

The authors would like to express their gratitude to Prof. Andrea Neto for his constructive criticism and insightful comments on the presented research. In addition, they would like to extend their thanks to the (anonymous) reviewers for their careful reading of the manuscript and their helpful suggestions for the improvement of this article.

REFERENCES

[1] N. Marcuvitz, "On field representations in terms of leaky modes or eigenmodes," *IRE Trans. Antennas Propag.*, vol. 4, no. 3, pp. 192–194, Jul. 1956.
[2] T. Tamir and A. A. Oliner, "Guided complex waves. Part 1: Fields at an interface," *Proc. IEE*, vol. 110, no. 2, pp. 310–324, 1963.
[3] H. Blok, J. M. Splunter, and H. G. Janssen, "Leaky-wave modes and their role in the numerical evaluation of the field excited by a line source in a non-symmetric, inhomogeneously layered, slab waveguide," *Appl. Sci. Res.*, vol. 41, nos. 3–4, pp. 223–236, 1984.
[4] K. A. Michalski and D. Zheng, "Rigorous analysis of open microstrip lines, of arbitrary cross section in bound and leaky regimes," *IEEE Trans. Microw. Theory Techn.*, vol. 37, no. 12, pp. 2005–2010, Dec. 1989.
[5] F. Mesa, C. Di Nallo, and D. R. Jackson, "The theory of surface-wave and space-wave leaky-mode excitation on microstrip lines," *IEEE Trans. Microw. Theory Techn.*, vol. 47, no. 2, pp. 207–215, Feb. 1999.
[6] A. Neto and S. Maci, "Green's function for an infinite slot printed between two homogeneous dielectrics. I. Magnetic currents," *IEEE Trans. Antennas Propag.*, vol. 51, no. 7, pp. 1572–1581, Jul. 2003.
[7] G. Lovat, P. Burghignoli, and D. R. Jackson, "Fundamental properties and optimization of broadside radiation from uniform leaky-wave antennas," *IEEE Trans. Antennas Propag.*, vol. 54, no. 5, pp. 1442–1452, May 2006.
[8] D. R. Jackson, C. Caloz, and T. Itoh, "Leaky-wave antennas," *Proc. IEEE*, vol. 100, no. 7, pp. 2194–2206, Jul. 2012.
[9] F. Monticone and A. Alù, "Leaky-wave theory, techniques, and applications: From microwaves to visible frequencies," *Proc. IEEE*, vol. 103, no. 5, pp. 793–821, May 2015.
[10] R. E. Collin, *Field Theory of Guided Waves*, 2nd ed. Piscataway, NJ, USA: IEEE Press, 1990.
[11] L. B. Felsen and F. Niu, "Spectral analysis and synthesis options for short pulse radiation from a point dipole in a grounded dielectric layer," *IEEE Trans. Antennas Propag.*, vol. 41, no. 6, pp. 747–754, Jun. 1993.
[12] D. G. Duffy, "Response of a grounded dielectric slab to an impulse line source using leaky modes," *IEEE Trans. Antennas Propag.*, vol. 42, no. 3, pp. 340–346, Mar. 1994.
[13] G. W. Hanson, A. B. Yakovlev, and J. Hao, "Leaky-wave analysis of transient fields due to sources in planarly layered media," *IEEE Trans. Antennas Propag.*, vol. 51, no. 2, pp. 146–159, Feb. 2003.
[14] D. G. Duffy, *Green's Functions With Applications*. Boca Raton, FL, USA: CRC Press, 2001.
[15] A. T. de Hoop, "A modification of Cagniard's method for solving seismic pulse problems," *Appl. Sci. Res., B*, vol. 8, pp. 349–356, Dec. 1960.
[16] M. Štumpf, A. T. de Hoop, and G. A. E. Vandenbosch, "Generalized ray theory for time-domain electromagnetic fields in horizontally layered media," *IEEE Trans. Antennas Propag.*, vol. 61, no. 5, pp. 2676–2687, May 2013.
[17] A. T. de Hoop and J. H. M. T. van der Hijden, "Generation of acoustic waves by an impulsive line source in a fluid/solid configuration with a plane boundary," *J. Acoust. Soc. Amer.*, vol. 74, no. 1, pp. 333–342, Jul. 1983.
[18] J. H. M. T. van der Hijden, "Quantitative analysis of the pseudo-Rayleigh phenomenon," *J. Acoust. Soc. Amer.*, vol. 75, no. 4, pp. 1041–1047, 1984.
[19] V. L. Ginzburg, "Radiation by uniformly moving sources (Vavilov–Cherenkov effect, transition radiation, and other phenomena)," *Phys.-Uspekhi*, vol. 39, no. 10, pp. 973–982, 1996, doi: 10.1070/PU1996v039n10ABEH000171.
[20] I. Palócz and A. A. Oliner, "Leaky space-charge waves I: Čerenkov radiation," *Proc. IEEE*, vol. 53, no. 1, pp. 24–36, Jan. 1965.
[21] A. Neto, "UWB, non dispersive radiation from the planarly fed leaky lens antenna—Part 1: Theory and design," *IEEE Trans. Antennas Propag.*, vol. 58, no. 7, pp. 2238–2247, Jul. 2010.

[22] A. T. de Hoop, "Pulsed electromagnetic radiation from a line source in a two-media configuration," *Radio Sci.*, vol. 14, no. 2, pp. 253–268, Mar./Apr. 1979.
[23] B. J. Kooij, "Transient Čerenkov radiation emitted by a pulsed line current traveling above the interface of a two-media configuration," in *IEEE Antennas Propag. Soc. Int. Symp. Dig.*, vol. 2, Jul. 1996, pp. 856–859.
[24] A. T. de Hoop, "Line-source excited pulsed acoustic wave reflection against the mass-loaded boundary of a fluid," in *AIP Conf. 3rd Conf. Math. Modeling Wave Phenomena*, vol. 1106, no. 1, Växjö, Sweden, 2009, pp. 118–129.
[25] M. Štumpf, A. T. de Hoop, and I. E. Lager, "Pulsed electromagnetic field radiation from a narrow slot antenna with a dielectric layer," *Radio Sci.*, vol. 45, no. 5, pp. 1–9, 2010.
[26] A. T. de Hoop, M. Štumpf, and I. E. Lager, "Pulsed electromagnetic field radiation from a wide slot antenna with a dielectric layer," *IEEE Trans. Antennas Propag.*, vol. 59, no. 8, pp. 2789–2798, Aug. 2011.
[27] J. Galejs, "Excitation of slots in a conducting screen above a lossy dielectric half space," *IRE Trans. Antennas Propag.*, vol. 10, no. 4, pp. 436–443, Jul. 1962.
[28] A. T. de Hoop, *Handbook of Radiation and Scattering of Waves*. London, U.K.: Academic, 1995.
[29] M. Štumpf, "Time-domain electromagnetic scattering by a two-dimensional narrow groove—A solution based on the Cagniard–DeHoop method of moments," *IEEE Antennas Wireless Propag. Lett.*, vol. 21, no. 3, pp. 586–589, Mar. 2022.
[30] M. Štumpf, *Time-Domain Electromagnetic Reciprocity in Antenna Modeling*. Hoboken, NJ, USA: Wiley, 2019.
[31] M. Abramowitz and I. A. Stegun, *Handbook of Mathematical Functions*. New York, NY, USA: Dover, 1972.
[32] M. Štumpf, *Metasurface Electromagnetics: The Cagniard–DeHoop Time-Domain Approach*. London, U.K.: IET, 2022.
[33] J. Gu, R. van Krieken, M. Štumpf, and I. E. Lager, "Excitation in time-domain analyses: A pivotal element for accurate simulations," in *Proc. 52nd Eur. Microw. Conf. (EuMC)*, Sep. 2022, pp. 234–237.
[34] M. Štumpf, G. Antonini, and I. E. Lager, "Pulsed electromagnetic excitation of a narrow slot between two dielectric halfspaces," *IEEE Trans. Antennas Propag.*, early access, Dec. 7, 2022, doi: 10.1109/TAP.2022.3226341.
[35] K. Aki and P. G. Richards, *Quantitative Seismology*, 2nd ed. Sausalito, CA, USA: Univ. Science Books, 2009.
[36] W. C. Chew, *Waves and Fields in Inhomogeneous Media*. Piscataway, NJ, USA: IEEE Press, 1995.
[37] G. F. Carrier and C. E. Pearson, *Partial Differential Equations: Theory and Technique*. New York, NY, USA: Academic, 1976.
[38] N. V. Budko, "Observation of locally negative velocity of the electromagnetic field in free space," *Phys. Rev. Lett.*, vol. 102, no. 2, Jan. 2009, Art. no. 020401.

Martin Štumpf (Senior Member, IEEE) received the Ph.D. degree in electrical engineering from the Brno University of Technology (BUT), Brno, Czech Republic, in 2011.

After his Ph.D. research, he spent a year and a half as a Post-Doctoral Fellow with KU Leuven, Leuven, Belgium. During a three-month period in 2018, he was a Visiting Professor at the UAq EMC Laboratory, University of L'Aquila, L'Aquila, Italy. He is currently an Associate Professor of theoretical electrical engineering with the Lerch Laboratory of EM Research, BUT. He has authored the books "*Electromagnetic Reciprocity in Antenna Theory*" (Wiley–IEEE Press, 2017), "*Pulsed EM Field Computation in Planar Circuits: The Contour Integral Method*" (CRC Press, 2018), "*Time-Domain Electromagnetic Reciprocity in Antenna Modeling*" (Wiley–IEEE Press, 2019), and "*Metasurface Electromagnetics: The Cagniard-DeHoop Time-Domain Approach*" (IET, 2022). His main research interests include modeling of electromagnetic wave phenomena with an emphasis on antenna theory and EMC.

Junhong Gu (Student Member, IEEE) was born in Weihai, Shandong, China, in December 3, 1997. He received the B.Sc. degree in electrical and electronic engineering from the University of Liverpool, Liverpool, U.K., in 2020, and the M.Sc. degree from the Terahertz Sensing Group, Delft University of Technology (TUDelft), Delft, The Netherlands, in 2022.

His research interests include applied electromagnetics, time-domain analysis of electromagetic wave phenomena, and the design of radio frequency power amplifier circuit and travelling-wave parametric amplifier circuit.

Ioan E. Lager (Senior Member, IEEE) received the Ph.D. degree in electrical engineering from the Delft University of Technology, Delft, The Netherlands, and the Transilvania University of Braşov, Braşov, Romania, in 1996.

He successively occupied research and academic positions with the Transilvania University of Braşov and the Delft University of Technology, where he is currently an Associate Professor. In 1997, he was a Visiting Scientist with Schlumberger-Doll Research, Ridgefield, CT, USA. He endeavors towards bridging the gap between electromagnetic field theory and the design, implementation, and measurement of antenna front-end architectures. His research interests include applied electromagnetics, especially time-domain propagation and applications, and antenna engineering, with an emphasis on nonperiodic (interleaved) array antenna architectures.